



Review

Recent Advances in CuInS₂-Based Photocathodes for Photoelectrochemical H₂ Evolution

Noyoung Yoon ^{1,2}, Oh Shim Joo ¹, Sang Youn Chae ^{3,4,*} and Eun Duck Park ^{3,5,*} ¹ Clean Energy Research Center, Korea Institute of Science and Technology, Seoul 02792, Republic of Korea² Department of Chemical and Biomolecular Engineering, Yonsei University, Seoul 03722, Republic of Korea³ Department of Energy Systems Research, Ajou University, Suwon 16499, Republic of Korea⁴ Institute of NT-IT Fusion Technology, Ajou University, Suwon 16499, Republic of Korea⁵ Department of Chemical Engineering, Ajou University, Suwon 16499, Republic of Korea

* Correspondence: sychae@ajou.ac.kr (S.Y.C.); edpark@ajou.ac.kr (E.D.P.); Tel.: +82-31-219-2384 (E.D.P.)

Abstract: Photoelectrochemical (PEC) H₂ production from water using solar energy is an ideal and environmentally friendly process. CuInS₂ is a p-type semiconductor that offers many advantages for PEC H₂ production. Therefore, this review summarizes studies on CuInS₂-based PEC cells designed for H₂ production. The theoretical background of PEC H₂ evolution and properties of the CuInS₂ semiconductor are initially explored. Subsequently, certain important strategies that have been executed to improve the activity and charge-separation characteristics of CuInS₂ photoelectrodes are examined; these include CuInS₂ synthesis methods, nanostructure development, heterojunction construction, and cocatalyst design. This review helps enhance the understanding of state-of-the-art CuInS₂-based photocathodes to enable the development of superior equivalents for efficient PEC H₂ production.

Keywords: copper indium sulfide; photoelectrochemical cell; hydrogen evolution reaction; heterojunction; cocatalyst



Citation: Yoon, N.; Joo, O.S.; Chae, S.Y.; Park, E.D. Recent Advances in CuInS₂-Based Photocathodes for Photoelectrochemical H₂ Evolution. *Nanomaterials* **2023**, *13*, 1361. <https://doi.org/10.3390/nano13081361>

Academic Editor: Narcis Homs

Received: 7 March 2023

Revised: 5 April 2023

Accepted: 11 April 2023

Published: 14 April 2023



Copyright: © 2023 by the authors. Licensee MDPI, Basel, Switzerland. This article is an open access article distributed under the terms and conditions of the Creative Commons Attribution (CC BY) license (<https://creativecommons.org/licenses/by/4.0/>).

1. Introduction

The use of renewable energy to reduce greenhouse gas emissions and environmental problems caused by fossil fuels is attracting considerable attention [1]. However, the intermittent nature of renewable energy necessitates the use of diverse energy storage systems. In particular, hydrogen is a promising, environmentally friendly, and carbon-neutral energy resource that emits only water while providing energy [2]. Hydrogen can be utilized in various systems, such as gas turbines, combustors, internal combustion engines, and fuel cells. However, CO₂-emitting fossil fuels are primarily being used to produce hydrogen owing to the economic feasibility of this strategy, thereby preventing the realization of a carbon-neutral society. In contrast, the production of hydrogen and oxygen through water splitting using renewable solar energy is an ideal method for storing solar energy in chemical form. Photoelectrochemical (PEC) water splitting is a representative method for converting solar light into chemical energy. PEC cells comprise a semiconductor photoelectrode, a counter electrode, and an electrolyte. When photons are absorbed by the photocatalytic electrode, photo-excited electron-hole pairs drive the water-splitting reaction ($\text{H}_2\text{O}(\text{l}) \rightarrow \text{H}_2(\text{g}) + 1/2\text{O}_2(\text{g})$, $\Delta H_{f,298\text{K}}^0 = -285.8 \text{ kJ/mol}$). However, the commercialization of PEC hydrogen production technology is hindered by its low solar-to-hydrogen conversion efficiency [3]. Therefore, the efficiency of PEC energy conversion must be improved.

A PEC cell is an ideal and environmentally friendly system for producing hydrogen via water photolysis, similar to photosynthesis in nature. Unlike photocatalytic water splitting, PEC water splitting does not require the separation of the generated hydrogen

and oxygen. Moreover, PEC cells have theoretically been predicted to achieve high solar-to-hydrogen conversion efficiencies depending on a single photo absorber or tandem configuration system (10–30%) [4]. In particular, the semiconductor photoelectrode is the most important part of PEC cells, as it interacts with photons and converts them into other forms of energy via charge-carrier excitation. Therefore, semiconductor materials suitable for photoelectrodes must be developed to increase the efficiency of the PEC reaction [5].

When semiconductor electrodes are in contact with electrolytes, the semiconductor experiences band bending owing to equilibration between the Fermi level of the semiconductor and the redox potential of the liquid. Under this band-bending condition, a depletion layer is formed, and a built-in potential is generated. When a semiconductor–liquid interface is irradiated with light, photons are absorbed by the semiconductor, and excited electron–hole pairs are subsequently generated. The electron–hole pairs are separated by the built-in potential; the electrons reduce the chemical species, and the holes oxidize the chemical species separately. In the case of n-type semiconductors, holes are transported into the semiconductor–liquid interface, producing oxygen, whereas in p-type semiconductors, electrons are transported into the semiconductor–liquid interface, producing hydrogen (Figure 1).

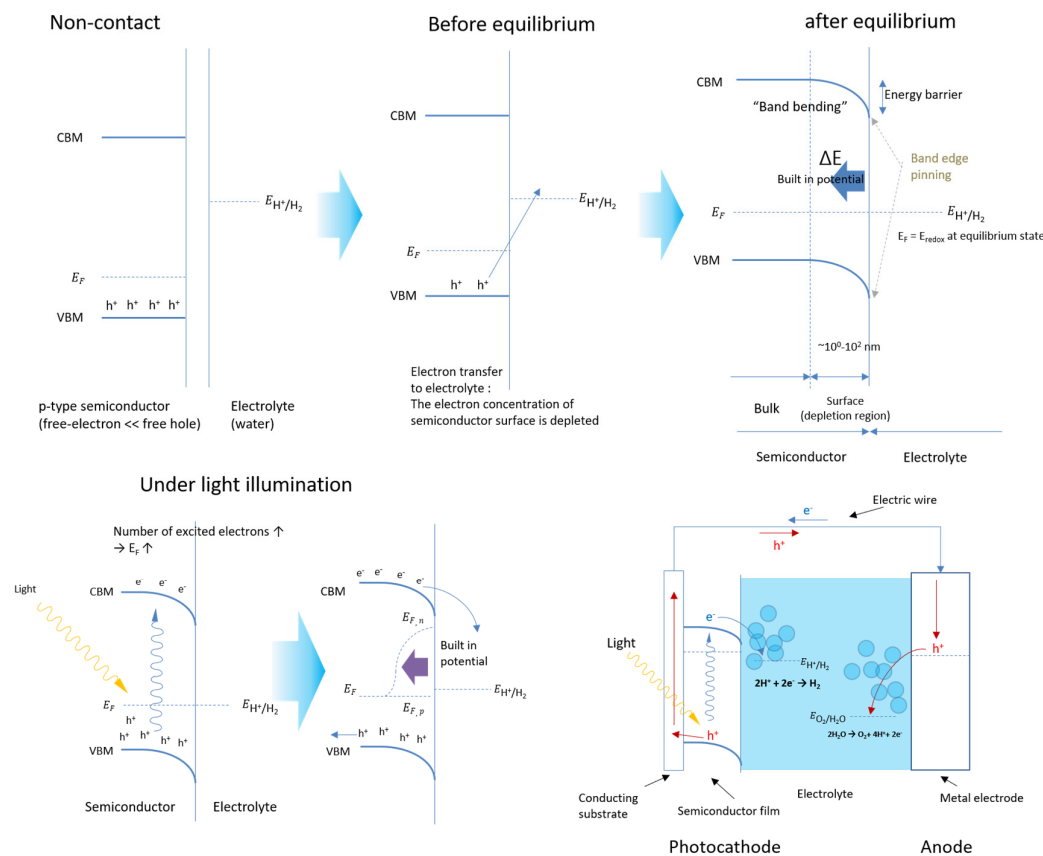


Figure 1. Band bending of p-type semiconductors in electrolytes. When the semiconductor and electrolyte are contacted, the Fermi level of the semiconductor and the chemical potential of the electrolyte become equilibrated and lead to a ‘band-bending energy’ structure. Under the light illumination condition, the excess photo-excited charge carrier breaks the equilibrium state and leads to charge separation via built-in potential at the semiconductor–electrolyte interface. A schematic of a photoelectrochemical (PEC) cell with a p-type semiconductor photocathode is also depicted for water splitting. Photo-excited electron is transported to the semiconductor/electrolyte interface, while the photo-excited hole is transported to the counter electrode through electrical wire and then to the counter electrode–electrolyte interface.

Efficient PEC water-splitting reactions with semiconductor materials can occur under various conditions. First, the bandgap of semiconductor materials should be smaller than 3.0 eV for the efficient utilization of visible solar light. Second, the bandgap must be higher than 1.23 eV to generate a sufficient driving force for the water-splitting reaction. Third, the band position (that is, the energy levels of the conduction and valence bands) should be located at a suitable level compared to the redox potential of water. The conduction band of the semiconductor should have a higher energy level than that of HER, while the valence band of the semiconductor should have a lower energy level than that of OER. Additionally, the semiconductor material should be free from photo-corrosion during the PEC reactions, or the semiconductor should be protected by a passive layer from corrosion [6].

Figure 2 shows the bandgaps and band positions of commonly investigated semiconductors. However, semiconductors that can utilize visible solar light, exhibit PEC stability, and spontaneously decompose water without an external potential have not yet been reported. Therefore, various strategies have been attempted to resolve these shortcomings of semiconductor photoelectrodes.

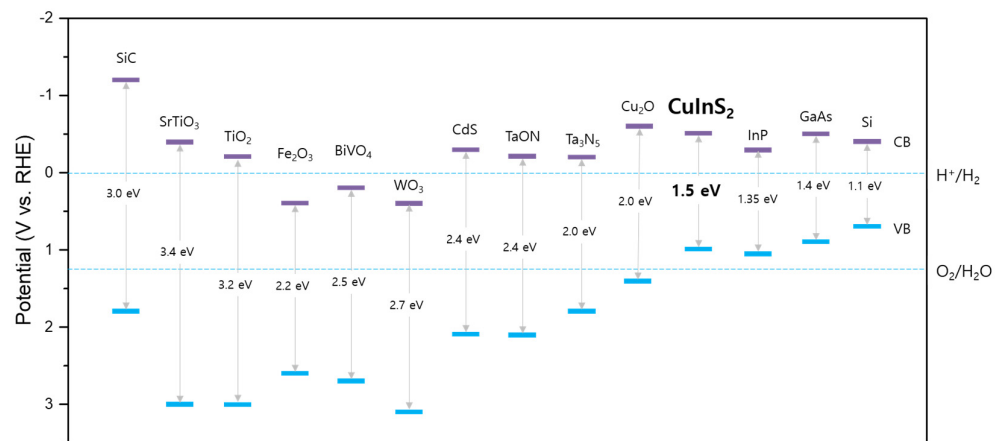


Figure 2. Bandgap and band position of various semiconductors.

Among the reported semiconductor materials, chalcopyrites are attractive photocatalytic substances appropriate for PEC hydrogen production. Chalcopyrites are semiconductors with the chemical composition ABX_2 and have a high absorption coefficient. Additionally, their band position is suitable for the hydrogen evolution reaction (HER). In particular, Cu-based chalcopyrite composites ($A = \text{Cu}$ or Ag ; $B = \text{In}$, Ga , or Al ; $X = \text{S}$ or Se) have a significantly high absorption coefficient ($\sim 10^5 \text{ cm}^{-1}$) owing to their direct bandgap structure, resulting in superior light-absorption characteristics compared to those of other semiconductor materials (Figure 3) [7]. Moreover, the bandgap of chalcopyrites can be easily adjusted (1.1–2.5 eV) by forming a solid solution via the replacement of the same-group atoms in the crystal lattice [8]. Furthermore, the higher level of the chalcopyrite conduction band allows excited electrons to have sufficient energy for driving the HER.

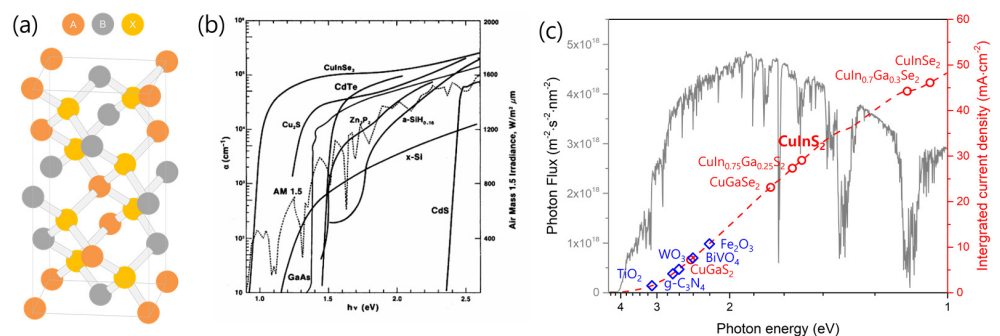


Figure 3. (a) Chalcopyrite unit-cell. (b) Absorption coefficient of various semiconductor materials [9].

(c) Bandgap of chalcopyrite semiconductors and other semiconductor materials. Integrated photocurrent density under 1.5 AM illumination was calculated based on band gap of semiconductors. Reproduced from ref. [9] with permission of the American Physical Society.

In this review, research trends in the use of photocathodes based on CuInS₂—a noteworthy chalcopyrite semiconductor—for PEC hydrogen evolution are surveyed. CuInS₂ has attractive properties, such as a suitable band position and bandgap for photocatalytic electrodes. Moreover, it is an economical chalcopyrite because it does not comprise relatively expensive elements, such as Ag, Ga, and Se. Additionally, it can be synthesized using economical methods, such as non-vacuum-based electrodeposition, solvothermal processes, and screen-printing techniques. Although concerns related to indium resource depletion exist, the amount of indium in the Earth's crust is sufficient for solar energy conversion and industrial applications [10].

The advantageous physical properties of CuInS₂ permit PEC hydrogen production. Because CuInS₂ has a bandgap of ~1.5 eV, which enables solar light absorption over an extremely wide range (from ultraviolet to near-infrared) and a high extinction coefficient (>10⁵ cm⁻¹) [11], it has been used in solar energy conversion systems, such as solar cells and photocatalysts, for a long time [12–15]. Although CuInS₂ generally exhibits p-type semiconductor characteristics, it can also attain n-type semiconductor attributes through the control of Cu vacancies or dopants [16–18]. However, in most studies on PEC cells, CuInS₂ is used as a p-type semiconductor and as a photocathode for hydrogen evolution. Despite having an excellent light-absorption ability, CuInS₂-based photoelectrodes generate a photocurrent of ~16 mA·cm⁻², which is approximately half of the theoretical photocurrent (~28.96 mA·cm⁻²) predicted from the bandgap (1.55 eV). Table 1 summarizes the activity of CuInS₂ photocathodes reported to date for PEC hydrogen evolution in terms of the photocurrent density, onset potential, and half-cell applied-bias photon-to-current conversion efficiency (HC-ABPE). The activity of CuInS₂ remains restricted by the high recombination of photogenerated electron–hole pairs, a surface state, inferior electrochemical catalytic properties, and low photochemical stability [19,20].

Table 1. Activity of CuInS₂-based photocathodes for PEC hydrogen evolution.

Photoelectrode	Substrate	Film Morphology	CuInS ₂ Synthesis Method	Current Density (mA·cm ⁻²)	Onset Potential (V _{RHE})	HC-ABPE ¹ (%)	Electrolyte	Ref.
CuInS ₂	Mo foil	Thin film	Co-electrodeposition/sulfurization	−0.75	0.18	−	0.1 M Eu(NO ₃) ₃ (pH 2.3)	[21]
CuInS ₂	Mo/glass	Thin film	Electrodeposition/sulfurization	−7 at −0.4 V _{Ag/AgCl}	−0.2 V _{Ag/AgCl}	−	0.2 M Eu(NO ₃) ₃	[22]
CuInS ₂	Mo/glass	Thin film	Spray pyrolysis/sulfurization	−2.3 at −0.4 V _{Ag/AgCl}	0.15 V _{Ag/AgCl}	−	0.1 M Eu(NO ₃) ₃ (pH 4)	[23]
CuInS ₂	ITO/glass ²	Network-like nanostructure	Hydrothermal method	−0.4 at −0.4 V _{RHE}	0.1	−	0.1 M Na ₂ SO ₄ (pH 6.7)	[24]
CuInS ₂	FTO/glass ³	Nanosheet arrays	Solvothermal/sputtering	−0.05	0.5	−	1.0 M KCl	[25]
CuInS ₂	ITO/glass	Nanosheet	Solvothermal	−0.07	−0.05	−	1.0 M KCl (pH 5.97)	[26]
CuInS ₂	ITO/glass	Heterostructure	Hydrothermal	−0.2 at −0.4 V _{RHE}	0	−	0.1 M Na ₂ SO ₄	[27]
CuInS ₂	Cu foil	Nanowire arrays	Facile gas–solid reaction/solvothermal	−0.1	0.2	−	1.0 M KCl (pH 5.97)	[28]
CuInS ₂ /CdS	Cu foil	Nanowire arrays	Facile gas–solid reaction/solvothermal	−0.48	0.2	−	1.0 M KCl (pH 5.97)	[28]
CuInS ₂ /CdS	Cu mesh	Nanowire arrays	Gas–solid reaction/solvothermal	−0.3	0.05	−	1.0 M KCl (pH 5.97)	[29]
CuInS ₂ /CdS	FTO/glass	Nanocrystalline	Spin coating	−1.2	0.49	−	20 mM MV ²⁺ 0.5 M Na ₂ SO ₄	[30]

Table 1. Cont.

Photoelectrode	Substrate	Film Morphology	CuInS ₂ Synthesis Method	Current Density (mA·cm ⁻²)	Onset Potential (V _{RHE})	HC-ABPE ¹ (%)	Electrolyte	Ref.
CuInS ₂ /CdS/ZnS	Glass	Nanorod arrays	AAO template growth/sulfurization ⁴	−0.01	0.3	-	0.5 M Na ₂ SO ₄ (pH 10)	[31]
CuInS ₂ /CdS/(Ta,Mo) _x (O,S) _y	Mo/glass	Thin film	Electrodeposition/sulfurization	−12	0.55	-	0.1 M HClO ₄ (pH 1.07)	[32]
CuInS ₂ /g-C ₃ N ₄	Mo/glass	Thin film	Sputtering/sulfurization	−0.02	0.15	-	0.1 M H ₂ SO ₄ (pH 1)	[33]
CuInS ₂ /Ni-MoS _x	Mo/glass	Thin film	Electrodeposition/sulfurization	−9	0.4	0.68	0.5 M KP _i (pH 7)	[34]
CuInS ₂ /MoS _x	Mo/glass	Thin film	Electrodeposition/sulfurization	−9.99	0.36	0.9	0.1 M HClO ₄ (pH 0.92–0.96)	[35]
CuInS ₂ /SnS ₂	FTO/glass	Nanosheet	Hydrothermal	−1 at −0.45V _{RHE}	-	-	0.5 M Na ₂ SO ₄	[36]
CuInS ₂ /SnS ₂ /C ₆₀	FTO/glass	Nanosheet	Hydrothermal	−1.5 at −0.45V _{RHE}	-	-	0.5 M Na ₂ SO ₄	[36]
CuInS ₂ /TaO _x	Mo/glass	Thin film	Electrodeposition/sulfurization	−9	0.2	-	0.5 M H ₂ SO ₄ (pH 0.35–39)	[20]
CuInS ₂ /Pt	Mo/glass	Thin film	Electrodeposition/sulfurization	−9.2	0.24	0.48	0.5 M KP _i (pH 7)	[34]
CuInS ₂ /Pt	Mo/glass	Thin film	Electrodeposition/sulfurization	−10.97	0.27	0.49	0.1 M HClO ₄ (pH 0.92–0.96)	[35]
CuInS ₂ /Ru	Mo/glass	Thin film	Electrodeposition/sulfurization	−8.02	0.15	0.25	0.1 M HClO ₄ (pH 0.92–0.96)	[35]
CuInS ₂ /Au	ITO/glass	Dotted disk	Wet chemical synthesis	−12	0.67	4.29	0.5 M Na ₂ SO ₄	[37]
CuInS ₂ /CdS-Pt	Mo/glass	Thin film	Electrodeposition/sulfurization	−15.12	0.5	1.6	0.1 M Na ₂ SO ₄ (pH 9)	[38]
CuInS ₂ /CdS-Pt	Mo/glass	Thin film	Electrodeposition/sulfurization	−11	0.55	1.8	0.2 M NaH ₂ PO ₄ (pH 6)	[39]
CuInS ₂ /CdS/Pt	Mo foil	Thin film	Electrodeposition/sulfurization	−7.5	0.6	-	0.2 M KH ₂ PO ₄ -Ar (pH 6.0)	[40]
CuInS ₂ /CdS/Pt	Mo/glass	Thin film	Electrodeposition/sulfurization	−13.4	0.58	2.3	0.5 M KP _i (pH 7)	[41]
CuInS ₂ /CdS/Pt	Mo/glass	Thin film	Electrodeposition/sulfurization	−8	0.5	1.06	0.1 M Na ₂ HPO ₄ (pH 10)	[42]
CuInS ₂ /CdS/TiO ₂ /Pt	Mo/glass	Thin film	Electrodeposition/sulfurization	−13	0.6	1.82	0.1 M Na ₂ HPO ₄ (pH 10)	[42]
CuInS ₂ /CdS/TaO _x /Pt	Mo/glass	Thin film	Electrodeposition/sulfurization	−16	0.55	-	0.1 M HClO ₄ (pH 1.07)	[32]
CuInS ₂ /CdS/AZO/TiO ₂ /Pt	FTO/glass	Thin film	Electrodeposition/solvothermal	−2	0.4	-	0.5 M Na ₂ SO ₄ 0.1 M KH ₂ PO ₄ (pH 5.0)	[43]
CuInS ₂ /In ₂ S ₃ -Pt	Mo/glass	Thin film	Electrodeposition/sulfurization	−15.16	0.6	1.9	0.1 M Na ₂ SO ₄ (pH 9)	[38]
CuInS ₂ /In ₂ S ₃ -Pt	Mo/glass	Thin film	Electrodeposition/sulfurization	−18	0.65	2.9	0.2 M NaH ₂ PO ₄ (pH 6)	[39]
CuInS ₂ /In ₂ S ₃ /Pt	Mo/glass	Thin film	Electrodeposition/sulfurization	−5.6	0.7	0.7	0.1 M Na ₂ SO ₄ (pH 10)	[44]
CuInS ₂ /In ₂ S ₃ /Pt	Mo/glass	Thin film	Co-electrodeposition/sulfurization	−5.2	0.5	0.83	0.25 M KH ₂ PO ₄ 0.25 M K ₂ HPO ₄ (pH 7)	[45]

Table 1. Cont.

Photoelectrode	Substrate	Film Morphology	CuInS ₂ Synthesis Method	Current Density (mA·cm ⁻²)	Onset Potential (V _{RHE})	HC-APBE ¹ (%)	Electrolyte	Ref.
CuInS ₂ /In ₂ S ₃ /Pt	FTO/glass	Thin film	Electrodeposition/sulfurization	−15	0.78	1.97	0.1 M Na ₂ SO ₄ (pH 9)	[46]
CuInS ₂ /Sb ₂ S ₃ /Pt	ITO/glass	Heterostructure	Hydrothermal	−0.2	0.4	-	0.1 M Na ₂ SO ₄	[27]
CuInS ₂ /MoS _x /Ru	Mo/glass	Thin film	Electrodeposition/sulfurization	−12.87	0.34	1.23	0.1 M HClO ₄ (pH 0.92–0.96)	[35]
CuInS ₂ /MoS _x /Pt	Mo/glass	Thin film	Electrodeposition/sulfurization	−14.82	0.33	1.08	0.1 M HClO ₄ (pH 0.92–0.96)	[35]
CuInS ₂ /Ni-MoS _x /Pt	Mo/glass	Thin film	Electrodeposition/sulfurization	−15.5	0.5	1.48	0.5 M KPi (pH 7)	[34]
CuInS ₂ /MoS _x O _y	Mo/glass	Thin film	Electrodeposition/sulfurization	−5.94	0.24	-	0.1 M HClO ₄ (pH 0.9–1.0)	[47]
CuInS ₂ /PNDI3OT-SeI/TiO ₂ /Pt	Mo/glass	Thin film	Electrodeposition/sulfurization	−15.67	0.25	1	0.1 M HClO ₄ (pH 0.9–1.0)	[48]
CuInS ₂ /PNDI3OT-Se ₂ /TiO ₂ /Pt	Mo/glass	Thin film	Electrodeposition/sulfurization	−4.91	0.15	0.15	0.1 M HClO ₄ (pH 0.9–1.0)	[48]
NaNbO ₃ /CuInS ₂	ITO/glass	Nanocube core/shell	Hydrothermal method	1.05 at −1 V _{Ag/AgCl}	−0.11 V _{Ag/AgCl}	-	0.5 M Na ₂ SO ₄	[49]
NaNbO ₃ /In ₂ S ₃ /CuInS ₂	ITO/glass	Nanocube core/shell	Hydrothermal method	1.63 at −1 V _{Ag/AgCl}	−0.11 V _{Ag/AgCl}	-	0.5 M Na ₂ SO ₄	[49]
NaNbO ₃ /CuInS ₂ /In ₂ S ₃	ITO/glass	Nanocube core/shell	Hydrothermal method	6.72 at −1 V _{Ag/AgCl}	−0.11 V _{Ag/AgCl}	-	0.5 M Na ₂ SO ₄	[49]
FeOOH/CuInS ₂ /Pt	ITO/glass	Nanoparticles	Successive ionic layer adsorption and reaction (SILAR)	−2	0.6	-	0.1 M Na ₂ SO ₄ (pH 7.1)	[50]
NiO/CuInS ₂	ITO/glass	Nanosheets	Hydrothermal	−0.23	0.2	-	0.1 M Na ₂ SO ₄	[51]
NiO/CuInS ₂ /NiS	ITO/glass	Nanosheets	Facial hydrothermal	−0.27	0.4	-	0.1 M Na ₂ SO ₄	[51]
(CuInS ₂) _{0.81} (ZnS) _{0.19} /CdS/Pt	Mo/glass		Electrodeposition/sulfurization	−16.7	0.84	5.6	0.5 M KPi (pH 7)	[41]

¹ HC-APBE: half-cell applied-bias photon-to-current conversion efficiency; ² ITO: indium tin oxide; ³ FTO: fluorine-doped tin oxide; ⁴ AAO: anodized aluminum oxide.

Therefore, methods for fabricating CuInS₂ photocathodes and strategies for improving their PEC performance are summarized and discussed in this review.

2. Synthesis Methods and Morphological Control Techniques for CuInS₂ Photocathodes

The synthesis methods for CuInS₂ thin films can be categorized into physical and chemical techniques. Sputtering and co-evaporation are representative physical methods that require ultrahigh-vacuum conditions, under which phase-pure chalcopyrite crystals with minimal impurities can be grown. Sputtering is a typical method for synthesizing CuInS₂ under vacuum conditions, in which Cu and In are sequentially deposited on substrates and converted into CuInS₂ through sulfurization. This method can produce thin films with excellent uniformity and readily controllable stoichiometries. However, the stipulated vacuum conditions lead to a remarkably high thin-film fabrication cost, increasing the unit cost of hydrogen production [52]. Therefore, wet chemical methods are being studied as an alternative CuInS₂ synthesis strategy (Figure 4).

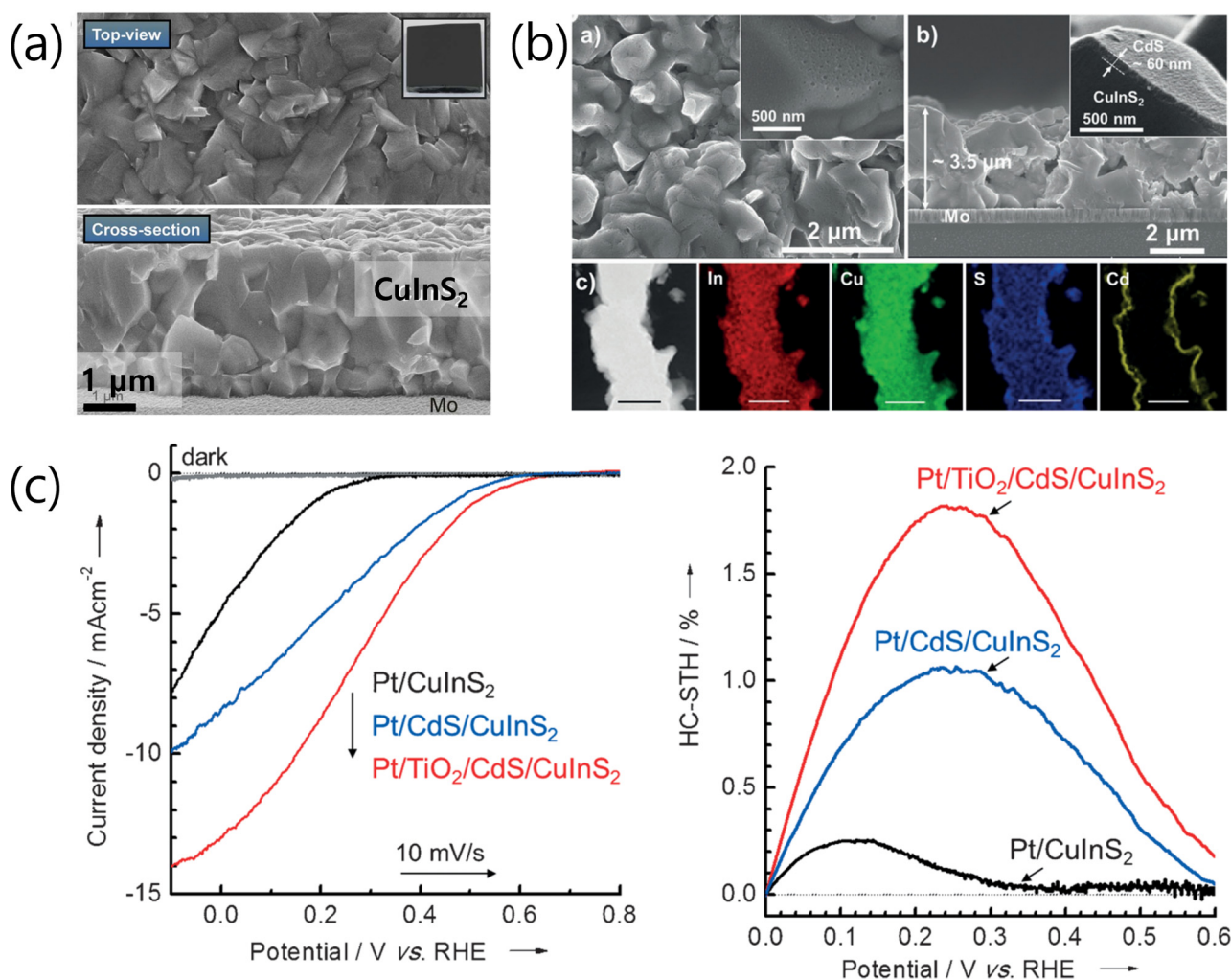


Figure 4. Crystal morphology of CuInS_2 thin films prepared by (a) sputtering [33] and (b) electrodeposition/sulfurization [42]. (c) Linear sweep voltammetry (LSV) profiles and HC-ABPE data of CuInS_2 -based photocathodes fabricated by electrodeposition/sulfurization [42]. Reproduced from ref. [29] with permission of the Royal Society of Chemistry. Reproduced from ref. [39] with permission from Wiley-VCH.

CuInS_2 can also be synthesized using solution-based approaches, such as chemical bath deposition, electrodeposition, spin coating, spray pyrolysis, and hydrothermal methods, which facilitate economical and large-scale preparation. Spin coating involves coating Cu/In precursor ink onto a rotating substrate. In this method, the Cu/In ratio can be easily controlled by adjusting the composition of the precursor solution; moreover, the thin-film thickness can be regulated by repetitive spin coating [53]. Spray pyrolysis, which involves spraying a precursor solution onto a high-temperature substrate, facilitates the preparation of large-area films. Here, the CuInS_2 composition can be adjusted using the concentration of the spray solution [23]. Electrodeposition–sulfurization is predominantly used to synthesize CuInS_2 photocathodes for PEC hydrogen evolution. Here, Cu and In are electrochemically deposited on conductive substrates in an electrolytic solution [42]. Co-deposition has also been performed to fabricate Cu–In alloy films [21]. Simultaneous electrodeposition of three elements can be performed in a Cu–In–S ternary electrolytic bath. Unlike other chalcopyrite materials, the CuInS_2 prepared by electrodeposition exhibits similar or even higher performance than that of the CuInS_2 photoelectrodes prepared by co-evaporation or sputtering. Therefore, electrodeposition is a promising technique for synthesizing high-performance CuInS_2 thin films (Figure 5).

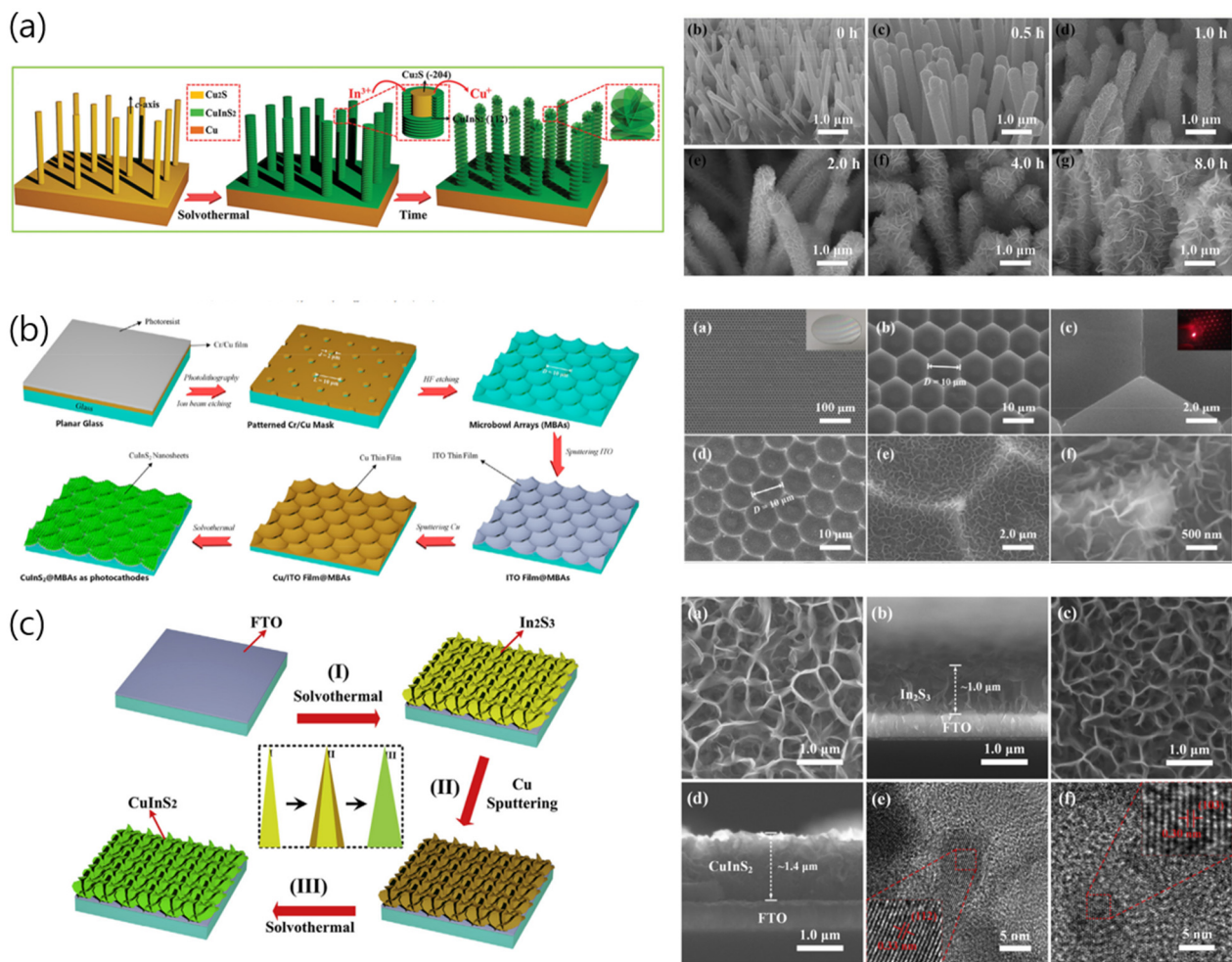


Figure 5. Schematics illustrating the preparation of various nanostructure-controlled CuInS_2 films and scanning electron microscopy (SEM) images of the films: (a) CuInS_2 nanorods array by facile gas–solid reaction/solvothermal [28], (b) photoelectrode based on 3D micro bowl arrays using CuInS_2 nanosheet array grown using solvothermal method as photocatalyst [26], and (c) CuInS_2 nanosheet arrays fabricated from In_2S_3 self-sacrificial templates using solvothermal and sputtering [25]. Reproduced from ref. [28] and ref. [26] with permission from Elsevier. Reproduced from ref. [25] with permission from Wiley-VCH.

However, the aforementioned methods are limited in terms of permitting nanostructural control to achieve high PEC activities. The multidimensional structure of semiconductor thin films is often critical to determining the PEC activity. One-dimensional (1D) nanostructures allow efficient PEC reactions owing to the improved charge separation/transport, and their unique optical and electrical properties lead to enhanced light absorption [31]. Additionally, most nanostructures exhibit higher light-trapping efficiencies and photocurrent densities than those of thin films of various materials. For example, photoelectrodes with structures such as nanowire arrays (NWAs), nanorod arrays, and nanotubes have the advantage of charge separation owing to the improved charge-carrier collection, rapid minority-carrier diffusion, and robustness of the electrode–electrolyte interface [31].

Three-dimensional branched nanoarray structures can improve the PEC performance of CuInS_2 photocathodes by enhancing their light-absorption characteristics and surface area. Moreover, two-dimensional structures can improve the PEC performance through enhancements in the electronic and optical properties and surface area. In particular, layered bonding is beneficial in terms of promoting photocarrier separation and improving the PEC performance by shortening the charge-transport duration and distance [28]. However, the

complex nature of multinary chalcogenide materials hinders the development of practical techniques for synthesizing vertically aligned structures. Most previously reported copper chalcopyrite nanostructures have been synthesized using hard nanoscale templates, such as anodic aluminum oxide (AAO). Yang et al. prepared CuInS₂ photocathodes with nanorod structures by impregnating AAO templates with a Cu/In precursor solution and used them for PEC hydrogen production [31]. The charge-carrier collection was found to be inefficient when the nanowire length was greater than the carrier-diffusion length (~1 μm). Additionally, the transport of photogenerated electrons to carrier collectors was suppressed as the surface area of CuInS₂ decreased with increasing nanowire diameter. Therefore, the 1D nanostructures had to be optimized in terms of diameter and length to maximize their advantages. Moreover, the control of the pores and depth of AAO templates have been reported to be key to preparing CuInS₂ nanorod arrays of an appropriate length. Hydrothermal/solvothermal approaches have also been implemented to adjust the CuInS₂ nanostructures [24,25,36]. Tu et al. deposited In₂S₃ nanosheet arrays on a fluorine-doped tin oxide (FTO) substrate using a solvothermal method and used them as self-sacrificing templates. Substantial CuInS₂ deposition was performed on the 2D structure, yielding 2D CuInS₂ nanosheets exhibiting strong excitonic effects, which led to an enhanced optoelectronic response and reduced radiative lifetime. This nanosheet array has the advantages of improved light collection and photogenerated charge pair creation [25].

3. Heterojunction Interface for CuInS₂

The low photovoltage generated by the rapid recombination of electron–hole pairs is a major factor that impedes photoelectrode activity [20]. In particular, the rate of hydrogen generation from CuInS₂ is significantly reduced, owing to its low photovoltage. However, the hydrogen production efficiency can be improved by creating a p–n junction between p-type CuInS₂ and n-type semiconductors [54].

Two types of p–n junctions exist—homojunctions and heterojunctions—which comprise the same and two different semiconductor materials, respectively. As they permit adjustment of the energy level that is matched with the bandgap between CuInS₂ and other semiconductor materials, p–n-type heterojunctions have been extensively used to suppress the recombination of electron–hole pairs in CuInS₂ photocathodes [34]. Among them, CdS is predominantly used for chalcopyrites and different p-type photoelectrodes (p-SnS, CdTe, and CuZnSnS₄) and is known to significantly improve photovoltage [54].

The difference in energy levels between two materials is particularly critical for enabling charge transfer at a heterojunction interface. The CuInS₂/CdS interface has a cliff-type heterojunction with a difference between conduction band levels of −0.47 eV. When excited electrons move from CuInS₂ to CdS through the conduction band, the energy difference (1.05 eV) between the conduction band of CdS and the valence band of CuInS₂ increases the recombination chance of electron–hole pairs at the interface. However, the CuInS₂–In₂S₃ interface has a notch-type energy structure when the heterojunction is formed. Moreover, the energy difference (1.79 eV) between the conduction band of In₂S₃ and the valence band of CuInS₂ is relatively larger than that of CuInS₂/CdS. Therefore, the electron–hole recombination is suppressed, and charges can be efficiently separated and transported to the reactant [39]. Owing to this difference in the energy structure, the CuInS₂/In₂S₃ photoelectrode (−18 mA·cm^{−2}) generates a higher photocurrent than that of CuInS₂/CdS (Figure 6).

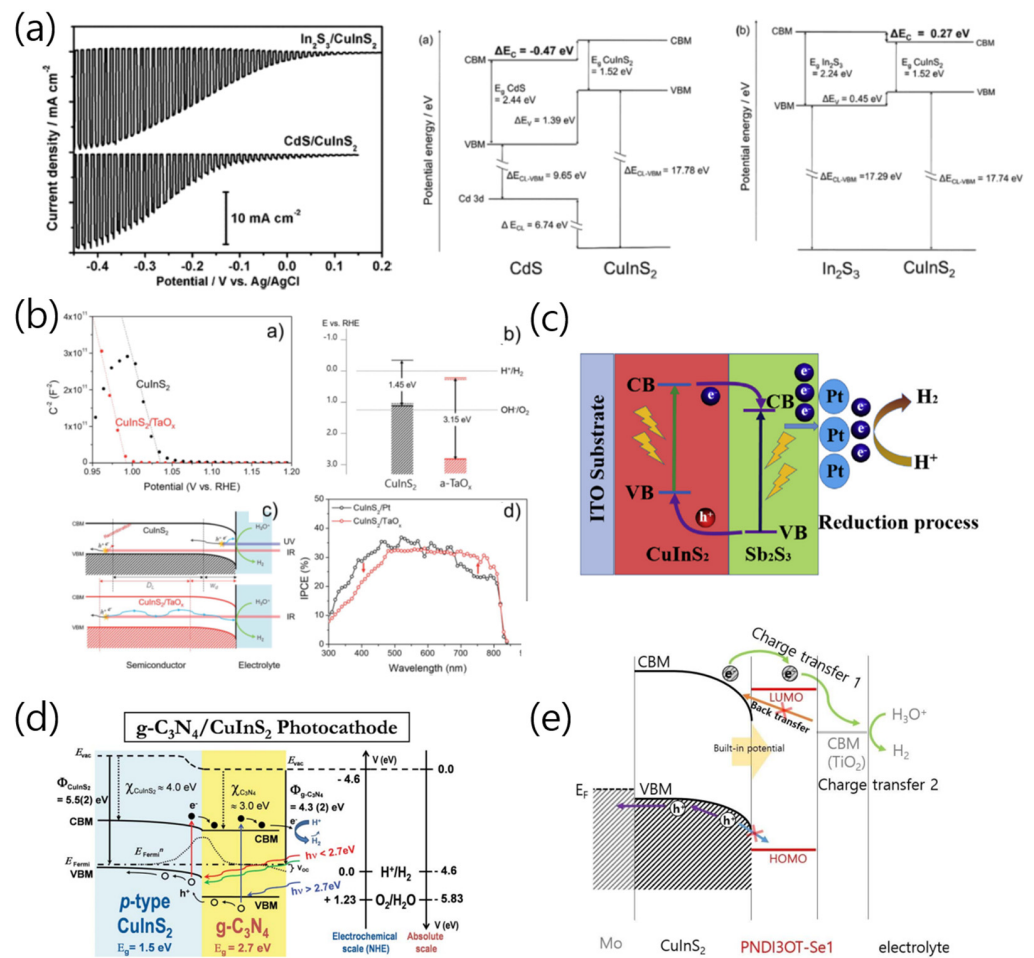


Figure 6. (a) Under chopped illumination of simulated sunlight (AM1.5), LSV profiles and difference in energy levels between CdS and In₂S₃ upon formation of a heterojunction with CuInS₂ for CuInS₂/CdS and CuInS₂/In₂S₃ photocathodes using an aqueous solution 0.2 M Eu(NO₃)₃ (pH 4) [39]. (b) Mott–Schottky plots of CuInS₂ and CuInS₂/TaO_x, Fermi-level shift of the CuInS₂/TaO_x heterojunction, a schematic diagram of band bending of CuInS₂ and CuInS₂/TaO_x photoelectrodes and incident-photon-to-electron conversion efficiency (IPCE) values for CuInS₂/TaO_x photocathodes [20]. (c) Schematic diagram of the CuInS₂/Sb₂S₃/Pt photoelectrodes. This band alignment indicates the charge-transfer process [27]. (d) Proposed energy band diagram of the CuInS₂/C₃N₄ [33]. (e) Schematic energy diagrams of CuInS₂/PNDI3OT-Se1-polymer heterojunctions, indicating charge transfer between semiconductors [48]. Reproduced from ref. [39] with permission from the American Chemical Society. Reproduced from ref. [20,33,48] with permission from the Royal Society of Chemistry. Reproduced from ref. [27] with permission from Elsevier.

MoS_x, Ni-MoS_x, SnS₂, Sb₂S₃, and TaO_x can also be used as n-type semiconductors for heterojunction formation with CuInS₂ photocathodes. MoS_x electrodeposited on CuInS₂ was found to generate an additional photovoltage of ~300 mV owing to p–n junction formation [35]. Moreover, Chae et al. found that the in situ transformation of crystalline MoS_x into amorphous MoS_x enhanced the charge transfer at the MoS_x/CuInS₂ interface, which improved the PEC HER activity [47]. Zhao et al. reported that Ni doping of MoS_x increased the PEC activity owing to the improved hydrogen evolution kinetics of MoS_x. The photocathode with the Ni-MoS_x/CuInS₂ heterojunction structure exhibited a higher onset potential (0.5 V_{RHE}) than that of bare CuInS₂ photocathodes [34].

The introduction of n-SnS₂ with a bandgap of 1.62 eV into CuInS₂ photoelectrodes can permit effective charge transfer owing to the energy-level difference between the two materials [36]. Similarly, at the interface between CuInS₂ and TaO_x, which is a multifunctional passive layer with lower conduction and valence bands than those of CuInS₂, electrons

and holes are efficiently transferred by a cliff-like energy-level structure similar to that of the $\text{CuInS}_2/\text{SnS}_2$ heterojunction. In particular, TaO_x has been observed to act as a multi-functional passivation layer that not only suppresses the recombination of electron–hole pairs but also increases the activity and stability for hydrogen production. Therefore, the incident-photon-to-electron conversion efficiency (IPCE) has been found to increase in longer-wavelength regions owing to the prolonged charge-carrier lifetime, resulting in a three-fold higher photocurrent than that of the CuInS_2 photoelectrodes [4].

Recently, atomically graded passivation layers were developed for CuInS_2 photocathodes. First, Mo:TaO_x layers were prepared by implanting Mo atoms into TaO_x layers. The resulting Mo:TaO_x film was then sulfurized, yielding a $(\text{Ta},\text{Mo})_x(\text{O},\text{S})_y$ layer. The graded distribution of Mo and S in the TaO_x matrix led to the synergetic PEC activity of CuInS_2 , similar to that of CuInS_2 photocathodes decorated with Pt cocatalysts [32]. n-Type polymer semiconductors could also be used to form p–n heterojunctions with CuInS_2 . When the n-type polymer semiconductor PNDI3OT-Se was deposited on CuInS_2 , the onset potential shifted, and the photocurrent increased, similar to that in an inorganic p–n junction, such as the $\text{CdS}/\text{CuInS}_2$ heterojunction [48]. The band position of PNDI3OT was adjusted using the monomer structure. Moreover, the valence band position of the polymer and CuInS_2 were critical for enabling efficient charge transfer at the polymer/ CuInS_2 interface. This result highlights the potential of polymer/inorganic hybrid photoelectrodes for realizing efficient hydrogen production.

4. Cocatalyst Decoration for Hydrogen Evolution

Even if photogenerated charges have a sufficient thermodynamic potential, they can easily recombine if the HER on the photoelectrode surface is kinetically unfavored. Poor kinetics at the semiconductor surface leads to a high overpotential; however, cocatalysts can reduce the activation energy, boosting the HER rate. Therefore, the HER rate of photocathodes can be improved by applying suitable cocatalysts onto the surface of semiconductor photoelectrodes. Noble metals are considered excellent electrocatalysts because of their high conductivity and low overpotential for the HER. Among noble and transition metals, Pt is known to be one of the best electrocatalysts for the HER. The activity trends can be explained using a ‘volcano plot’ showing the adsorption/desorption energy of hydrogen ions on the catalyst surface. Therefore, noble metals are extensively used as cocatalysts for photocathodes; however, their expensiveness necessitates the development of economical cocatalyst alternatives. For instance, relatively inexpensive transition metal cocatalysts or protective layers have been used to enhance the activity and stability of $\text{Cu}(\text{In},\text{Ga})\text{Se}_2$ (CIGS) photoelectrodes. Moreover, Ni–Mo cocatalysts have improved the stability and activity of CIGS photoelectrodes under neutral electrolyte conditions [55]. When a Ti–Mo layer was introduced between Pt cocatalysts and CIGS/ CdS electrodes, the stability and activity were significantly increased in neutral electrolytes [56]. However, several transition metals are unstable under low-pH conditions, which limits the use of strongly acidic electrolytes. Transition metal–sulfide cocatalysts (MoS_x , CoS_x , CoSe_x , and NiS_x) have exhibited high hydrogen-generation activity in chalcopyrite and Si photoelectrodes [57–62]. However, the development of cocatalysts for CuInS_2 photoelectrodes is lagging behind that of other chalcopyrite-based photoelectrodes, with Pt cocatalysts being used in most cases. Therefore, various HER cocatalysts must be applied to CuInS_2 -based photoelectrodes, and their activity and mechanism should be investigated (Figure 7).

Charge transfer at the photoelectrode–cocatalyst interface should also be the focus, along with the electrocatalytic activity of cocatalysts. Although Pt is experimentally and theoretically regarded as one of the best HER electrocatalysts, it may be unsuitable for application on photoelectrode surfaces. Patra et al. used Au nanoparticles as a cocatalyst with CuInS_2 particles, which significantly increased the hydrogen evolution activity owing to the smooth charge transport between CuInS_2 and Au through surface-Plasmon-resonance effects [37]. Chae et al. incorporated photoelectrodes with Ru, which has a lower production activity than that of Pt and achieved a high solar-to-hydrogen conversion efficiency [35].

The high work function of Ru induced effective charge transfer from $\text{CuInS}_2/\text{MoS}_x$ along with ohmic junction formation, whereas the $\text{CuInS}_2/\text{MoS}_x/\text{Pt}$ interface did not form an ohmic junction. Therefore, charge transfer at the cocatalyst– CuInS_2 interface must be considered for designing efficient cocatalysts.

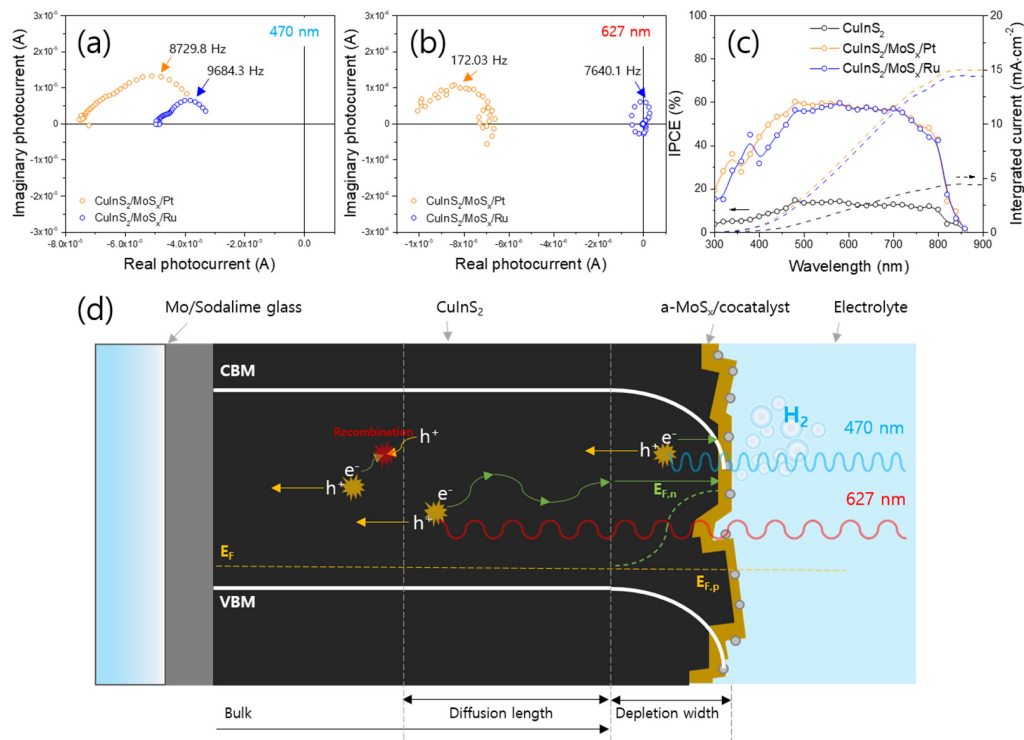


Figure 7. Effects of Ru and Pt cocatalysts on $\text{CuInS}_2/\text{MoS}_x$ photocathodes, such as the improved transient time of electrons by the Ru cocatalysts. Intensity-modulated photocurrent spectroscopy results of CuInS_2 -based photocathodes under (a) 470 nm and (b) 627 nm LED light. (c) IPCE data of CuInS_2 -based photocathodes. (d) Schematic diagram of charge carrier transportation at $\text{CuInS}_2/\text{MoS}_x/\text{cocatalysts}$ interfaces [35]. Reproduced from ref. [31] with permission from Elsevier.

5. Hole Transport Layers

Generally, holes in the p-type chalcopyrite semiconductor CuInS_2 —which are a majority carrier—have higher mobility and longer lifetimes than those of electrons [63]. Therefore, improving the electron transport/transfer in the semiconductor layer or at the semiconductor–electrolyte interface has received more attention than hole transportation. However, the enhancement of hole transfer has been found to be crucial for improving the activity of CuInS_2 . In most cases, CuInS_2 crystals have been grown on Mo foil or Mo-coated substrates because of the ohmic contact enabled between Mo and CuInS_2 (or other chalcopyrite materials) [64,65]. However, transparent substrates can be effective depending on the direction of illumination for determining the charge-transport property of photoelectrodes [66]. CuInS_2 films have been grown on transparent conductive substrates, such as glass coated with indium tin oxide (ITO) or fluorine-doped tin oxide (FTO), which have been extensively used for PEC cells. Liu et al. reported that FeOOH interlayers between CuInS_2 and ITO improved the hole transfer from CuInS_2 to the ITO layer, which led to the FTO/FeOOH/ CuInS_2/Pt photocathodes exhibiting a photoactivity 3.1 times higher than that of ITO/ CuInS_2 photocathodes [50]. FeOOH effectively captured excited holes owing to its hole-storing tendency, and the electron–hole pair recombination of CuInS_2 was suppressed. Kumar et al. synthesized $\text{NaNbO}_3/\text{CuInS}_2/\text{In}_2\text{S}_3$ and $\text{NaNbO}_3/\text{In}_2\text{S}_3/\text{CuInS}_2$ core/shell/shell nanocubes for PEC applications [49]. In the $\text{NaNbO}_3/\text{CuInS}_2/\text{In}_2\text{S}_3$ system, CuInS_2 and In_2S_3 exhibited z-scheme behavior; however, $\text{NaNbO}_3/\text{In}_2\text{S}_3/\text{CuInS}_2$ had a type II band structure. The z-scheme nanocube immobilized on ITO exhibited a

considerably higher photocurrent than that of the electrodes immobilized with the type-II-structured nanocube. This type of energy-level design may facilitate hole transfer at a non-ohmic interface between CuInS_2 and the transparent, conductive metal-oxide layer (ITO or FTO).

6. Solid Solutions of CuInS_2

Solid solutions of chalcopyrite CuInS_2 crystals and other atoms can be readily prepared. For example, various photocathode materials, such as $\text{Cu}(\text{In,Ga})\text{Se}_2$, CuGaSe_2 , $(\text{Ag,Cu})\text{GaSe}_2$, and $\text{CuIn}(\text{S,Se})_2$, have been studied for the HER [67–70]. However, the activity and physicochemical properties of this type of material are beyond the scope of this review. Nevertheless, the solid solution of chalcopyrite CuInS_2 and zincblende ZnS is worth mentioning. Zhao et al. prepared solid solution crystals of $(\text{CuInS}_2)_x(\text{ZnS})_{1-x}$ using an electrodeposition–sulfurization method [41]. The enlarged bandgap of the solid solution $(\text{CuInS}_2)_x(\text{ZnS})_{1-x}$ led to a significantly high onset potential (up to 0.8 V_{RHE}). The half-cell solar-to-hydrogen conversion efficiency of the $(\text{CuInS}_2)_x(\text{ZnS})_{1-x}/\text{CdS}/\text{Pt}$ photocathodes was 5.6%, which is a remarkably high value among CuInS_2 -based photocathodes. This result emphasizes the benefits of solid solutions containing CuInS_2 or other materials over those of the simple bilayer-structured equivalents because of the graded band structure obtained by the atomic gradation of the semiconductor.

7. Summary and Outlook

CuInS_2 -based photocathodes for PEC hydrogen evolution are reviewed herein, with a focus on their synthesis methods, heterolayer construction, and cocatalyst design. CuInS_2 has been synthesized using physical (co-evaporation and sputtering) and chemical techniques (electrodeposition, spin coating, spray pyrolysis, and hydrothermal methods). Generally, the physical methods yield a dense, high-quality chalcopyrite thin film with large grains and high crystallinity, with the highly crystalline semiconductors exhibiting high PEC activity. Therefore, the physical methods enable higher PEC performance than that of the solution-based methods. However, unlike other quaternary or pentanary chalcopyrite materials, CuInS_2 synthesized using electrodeposition methods has similar or superior PEC activity compared to that of CuInS_2 films prepared using physical methods. Additionally, certain solution-based methods offer advantages in controlling the morphological features of CuInS_2 , such as dimensions and porosity. However, the complex nanostructure can also have more defect sites than those in a highly crystallized thin film. The activity of CuInS_2 -based photoelectrodes synthesized to date using solvo(hydro)thermal or other solution-based methods is considerably inferior to that of specimens prepared by electrodeposition. Therefore, nanostructural control remains insufficient for overcoming the rapid charge recombination at the defect or surface states of the CuInS_2 crystal. A new solution-based synthesis method for CuInS_2 with high PEC activity remains to be developed.

The use of heterojunctions to suppress electron–hole recombination has been extensively studied. Many sulfide materials (CdS , In_2S_3 , ZnS , NiS_x , and MoS_x) have been investigated for constructing a heterojunction or p–n junction with CuInS_2 . Moreover, certain metal oxides, atomic-graded metal oxides, and n-type polymer semiconductors have also been introduced. The bandgap alignment between CuInS_2 and heteromaterials is critical to enabling efficient charge transfer at the interface. Suitable band energy matching can successfully suppress the electron–hole recombination, boosting the photocurrent and improving the onset potential.

Cocatalysts that can facilitate hydrogen evolution from a photoelectrode surface are also important. The CuInS_2 surface is kinetically unfavorable for the HER and thereby requires a cocatalyst to reduce the overpotential. Pt, which has been widely used as a cocatalyst for CuInS_2 -based photocathodes, should be replaced with economical and earth-abundant materials. Although certain noble metals and metal sulfides have been investigated as cocatalysts for CuInS_2 photoelectrodes, more diverse cocatalyst materials

should be examined. Additionally, when a cocatalyst is applied to a PEC system, the electrochemical activity of the cocatalyst, as well as the interfacial charge transfer between CuInS_2 and the cocatalyst, must be considered. Similarly, interfacial charge transfer between CuInS_2 and substrates can be controlled using hole-transporting interlayers. Finally, the use of a partial solid solution at the interface with CuInS_2 can be an effective strategy for enabling efficient charge transfer at several interfaces in a photoelectrode structure. All these strategies should be combined to achieve the theoretical limit of a PEC cell with a CuInS_2 photoelectrode.

Author Contributions: Writing—original draft preparation, N.Y. and S.Y.C.; writing—review and editing, O.S.J. and E.D.P.; supervision, E.D.P. All authors have read and agreed to the published version of the manuscript.

Funding: This study was supported by the institutional program of the Korea Institute of Science and Technology (KIST-2E32561). This work was supported by C1 Gas Refinery Program through the National Research Foundation of Korea (NRF) funded by the Ministry of Science, ICT, and Future Planning (2015M3D3A1A01064899). This research was supported by Basic Science Research Program through the National Research Foundation of Korea (NRF) funded by the Ministry of Education(2021R1A6A1A10044950).

Institutional Review Board Statement: Not applicable.

Informed Consent Statement: Not applicable.

Data Availability Statement: The data presented in this study are available in this article.

Conflicts of Interest: The authors declare no conflict of interest.

References

1. Wuebbles, D.J.; Jain, A.K. Concerns about climate change and the role of fossil fuel use. *Fuel Process. Technol.* **2001**, *71*, 99–119. [[CrossRef](#)]
2. Glenk, G.; Reichelstein, S. Economics of converting renewable power to hydrogen. *Nat. Energy* **2019**, *4*, 216–222. [[CrossRef](#)]
3. Grimm, A.; de Jong, W.A.; Kramer, G.J. Renewable hydrogen production: A techno-economic comparison of photoelectrochemical cells and photovoltaic-electrolysis. *Int. J. Hydrogen Energy* **2020**, *45*, 22545–22555. [[CrossRef](#)]
4. Chiu, Y.-H.; Lai, T.-H.; Kuo, M.-Y.; Hsieh, P.-Y.; Hsu, Y.-J. Photoelectrochemical cells for solar hydrogen production: Challenges and opportunities. *APL Mater.* **2019**, *7*, 080901. [[CrossRef](#)]
5. Sivula, K.; van de Krol, R. Semiconducting materials for photoelectrochemical energy conversion. *Nat. Rev. Mater.* **2016**, *1*, 15010. [[CrossRef](#)]
6. Scheuermann, A.G.; McIntyre, P.C. Atomic Layer Deposited Corrosion Protection: A Path to Stable and Efficient Photoelectrochemical Cells. *J. Phys. Chem. Lett.* **2016**, *7*, 2867–2878. [[CrossRef](#)]
7. Cao, Z.; Yang, S.; Wang, M.; Huang, X.; Li, H.; Yi, J.; Zhong, J. $\text{Cu}(\text{In,Ga})\text{S}_2$ absorber layer prepared for thin film solar cell by electrodeposition of Cu-Ga precursor from deep eutectic solvent. *Solar Energy* **2016**, *139*, 29–35. [[CrossRef](#)]
8. Tsoulka, P.; Rivalland, A.; Arzel, L.; Barreau, N. Improved CuGaSe_2 absorber properties through a modified co-evaporation process. *Thin Solid Films* **2020**, *709*, 138224. [[CrossRef](#)]
9. Jaffe, J.E.; Zunger, A. Theory of the band-gap anomaly in ABC_2 chalcopyrite semiconductors. *Phys. Rev. B* **1984**, *29*, 1882–1906. [[CrossRef](#)]
10. Werner, T.T.; Mudd, G.M.; Jowitt, S.M. The world's by-product and critical metal resources part III: A global assessment of indium. *Ore Geol. Rev.* **2017**, *86*, 939–956. [[CrossRef](#)]
11. Levchenko, S.; Syrbu, N.N.; Tezlevan, V.E.; Arushanov, E.; Doka-Yamigno, S.; Schedel-Niedrig, T.; Lux-Steiner, M.C. Optical spectra and energy band structure of single crystalline CuGaS_2 and CuInS_2 . *J. Phys. Condens. Matter* **2007**, *19*, 456222. [[CrossRef](#)]
12. Thirumalaisamy, L.; Palanivel, S.; Jeyakumar, K.; Kunjithapatham, S.; Watson, T.; Pitchaimuthu, S. The upsurge of absorption coefficient in CuInS_2 thin film with Ru doping: An energetic absorber layer in a superstrate solar cell. *Mater. Today Chem.* **2022**, *26*, 101217. [[CrossRef](#)]
13. Klenk, R.; Klaer, J.; Scheer, R.; Lux-Steiner, M.C.; Luck, I.; Meyer, N.; Rühle, U. Solar cells based on CuInS_2 —An overview. *Thin Solid Films* **2005**, *480–481*, 509–514. [[CrossRef](#)]
14. Tsuji, I.; Kato, H.; Kudo, A. Photocatalytic Hydrogen Evolution on $\text{ZnS}-\text{CuInS}_2-\text{AgInS}_2$ Solid Solution Photocatalysts with Wide Visible Light Absorption Bands. *Chem. Mater.* **2006**, *18*, 1969–1975. [[CrossRef](#)]
15. Chumha, N.; Pudkon, W.; Chachvalvutikul, A.; Luangwanta, T.; Randorn, C.; Inceesungvorn, B.; Ngamjarrojana, A.; Kaowphong, S. Photocatalytic activity of CuInS_2 nanoparticles synthesized via a simple and rapid microwave heating process. *Mater. Res. Express* **2020**, *7*, 015074. [[CrossRef](#)]

16. Feng, X.; Li, R.; Wang, M.; Chen, Y. Switchable synthesis of p- and n-type Cu–In–S grooved pyramid-like microcrystals for unassisted photoelectrochemical water splitting. *J. Mater. Chem. A* **2018**, *6*, 11180–11188. [[CrossRef](#)]
17. Logu, T.; Sankarasubramanian, K.; Soundarrajan, P.; Sampath, M.; Sethuraman, K. Growth of N type CuInS₂ microspheres on P type CuInS₂ seed layer prepared using facile low cost chemical methods. *Superlattices Microstruct.* **2015**, *83*, 690–698. [[CrossRef](#)]
18. Courtel, F.M.; Hammami, A.; Imbeault, R.; Hersant, G.; Paynter, R.W.; Marsan, B.; Morin, M. Synthesis of n-type CuInS₂ Particles Using N-methylimidazole, Characterization and Growth Mechanism. *Chem. Mater.* **2010**, *22*, 3752–3761. [[CrossRef](#)]
19. Sood, M.; Bombsch, J.; Lomuscio, A.; Shukla, S.; Hartmann, C.; Frisch, J.; Bremsteller, W.; Ueda, S.; Wilks, R.G.; Bär, M.; et al. Origin of Interface Limitation in Zn(O,S)/CuInS₂-Based Solar Cells. *ACS Appl. Mater. Interfaces* **2022**, *14*, 9676–9684. [[CrossRef](#)]
20. Chae, S.Y.; Kim, S.; Joo, O.-S. Design of an amorphous TaO_x multifunctional interfacial layer on photocathodes for photoelectrochemical H₂ evolution. *J. Mater. Chem. A* **2019**, *7*, 2041–2047. [[CrossRef](#)]
21. Unveroglu, B.; Zangari, G. Formation of p-type CuInS₂ absorber layers via sulfurization of co-electrodeposited Cu–In precursors. *RSC Adv.* **2015**, *5*, 81642–81649. [[CrossRef](#)]
22. Gunawan; Haris, A.; Widiyandari, H.; Widodo, D.S. Effect of potentials and electric charges for copper and indium depositions to the photocurrent responses of CuInS₂ thin films fabricated by stack electrodeposition followed by sulfurization. *IOP Conf. Ser. Mater. Sci. Eng.* **2018**, *349*, 012074. [[CrossRef](#)]
23. Ikeda, S.; Nonogaki, M.; Septina, W.; Gunawan, G.; Harada, T.; Matsumura, M. Photoelectrochemical Characterizations of CuInS₂ and Cu(In,Ga)S₂ Thin Films Fabricated by a Spray Pyrolysis Method. *Adv. Mater. Res.* **2014**, *894*, 427–431. [[CrossRef](#)]
24. Cai, Q.; Liu, Z.; Ma, C.; Tong, Z.; Han, C. Network-like CuInS₂ photocathode and modified with noble metal co-catalyst for photoelectrochemical water splitting. *J. Mater. Sci. Mater. Electron.* **2018**, *29*, 20629–20638. [[CrossRef](#)]
25. Tu, X.; Li, M.; Su, Y.; Yin, G.; Lu, J.; He, D. Self-templated growth of CuInS₂ nanosheet arrays for photoelectrochemical water splitting. *J. Alloys Compd.* **2019**, *809*, 151794. [[CrossRef](#)]
26. Li, M.; Chen, L.; Su, Y.; Yin, H.; Hu, K. Hexagonally ordered microbowl arrays decorated with ultrathin CuInS₂ nanosheets for enhanced photoelectrochemical performance. *J. Energy Chem.* **2020**, *51*, 134–142. [[CrossRef](#)]
27. Cai, Q.; Liu, Z.; Han, C.; Tong, Z.; Ma, C. CuInS₂/Sb₂S₃ heterostructure modified with noble metal co-catalyst for efficient photoelectrochemical water splitting. *J. Alloys Compd.* **2019**, *795*, 319–326. [[CrossRef](#)]
28. Li, M.; Zhao, R.; Su, Y.; Hu, J.; Yang, Z.; Zhang, Y. Hierarchically CuInS₂ Nanosheet-Constructed Nanowire Arrays for Photoelectrochemical Water Splitting. *Adv. Mater. Interfaces* **2016**, *3*, 1600494. [[CrossRef](#)]
29. Li, M.; Zhao, R.; Su, Y.; Hu, J.; Yang, Z.; Zhang, Y. Synthesis of CuInS₂ nanowire arrays via solution transformation of Cu₂S self-template for enhanced photoelectrochemical performance. *Appl. Catal. B Environ.* **2017**, *203*, 715–724. [[CrossRef](#)]
30. Amano, F.; Ebina, T.; Ohtani, B. Photoelectrochemical Hydrogen Evolution Using Copper-Indium-Sulfide Nanocrystalline Film Electrodes. *Electrochemistry* **2011**, *79*, 804–806. [[CrossRef](#)]
31. Yang, W.; Oh, Y.; Kim, J.; Kim, H.; Shin, H.; Moon, J. Photoelectrochemical Properties of Vertically Aligned CuInS₂ Nanorod Arrays Prepared via Template-Assisted Growth and Transfer. *ACS Appl. Mater. Interfaces* **2016**, *8*, 425–431. [[CrossRef](#)] [[PubMed](#)]
32. Chae, S.Y.; Kim, Y.; Park, E.D.; Im, S.H.; Joo, O.-S. CuInS₂ Photocathodes with Atomic Gradation-Controlled (Ta,Mo)_x(O,S)_y Passivation Layers for Efficient Photoelectrochemical H₂ Production. *ACS Appl. Mater. Interfaces* **2021**, *13*, 58447–58457. [[CrossRef](#)] [[PubMed](#)]
33. Yang, F.; Kuznietsov, V.; Lublow, M.; Merschjann, C.; Steigert, A.; Klaer, J.; Thomas, A.; Schedel-Niedrig, T. Solar hydrogen evolution using metal-free photocatalytic polymeric carbon nitride/CuInS₂ composites as photocathodes. *J. Mater. Chem. A* **2013**, *1*, 6407–6415. [[CrossRef](#)]
34. Zhao, J.; Minegishi, T.; Ma, G.; Zhong, M.; Hisatomi, T.; Katayama, M.; Yamada, T.; Domen, K. Efficient photoelectrochemical hydrogen production over CuInS₂ photocathodes modified with amorphous Ni-MoS_x operating in a neutral electrolyte. *Sustain. Energy Fuels* **2020**, *4*, 1607–1611. [[CrossRef](#)]
35. Chae, S.Y.; Yoon, N.; Park, E.D.; Joo, O.S. Surface modification of CuInS₂ photocathodes with ruthenium co-catalysts for efficient solar water splitting. *Appl. Surf. Sci.* **2023**, *612*, 155856. [[CrossRef](#)]
36. Zhang, F.; Chen, Y.; Zhou, W.; Ren, C.; Gao, H.; Tian, G. Hierarchical SnS₂/CuInS₂ Nanosheet Heterostructure Films Decorated with C₆₀ for Remarkable Photoelectrochemical Water Splitting. *ACS Appl. Mater. Interfaces* **2019**, *11*, 9093–9101. [[CrossRef](#)]
37. Patra, B.K.; Khilari, S.; Pradhan, D.; Pradhan, N. Hybrid Dot–Disk Au–CuInS₂ Nanostructures as Active Photocathode for Efficient Evolution of Hydrogen from Water. *Chem. Mater.* **2016**, *28*, 4358–4366. [[CrossRef](#)]
38. Gunawan; Haris, A.; Widiyandari, H.; Septina, W.; Ikeda, S. Surface modifications of chalcopyrite CuInS₂ thin films for photocathodes in photoelectrochemical water splitting under sunlight irradiation. *IOP Conf. Ser. Mater. Sci. Eng.* **2017**, *172*, 012021. [[CrossRef](#)]
39. Gunawan; Septina, W.; Harada, T.; Nose, Y.; Ikeda, S. Investigation of the Electric Structures of Heterointerfaces in Pt- and In₂S₃-Modified CuInS₂ Photocathodes Used for Sunlight-Induced Hydrogen Evolution. *ACS Appl. Mater. Interfaces* **2015**, *7*, 16086–16092. [[CrossRef](#)]
40. Takashima, T.; Fujishiro, Y.; Irie, H. Noble Metal Modification of CdS-Covered CuInS₂ Electrodes for Improved Photoelectrochemical Activity and Stability. *Catalysts* **2020**, *10*, 949. [[CrossRef](#)]
41. Zhao, J.; Minegishi, T.; Kaneko, H.; Ma, G.; Zhong, M.; Nakabayashi, M.; Hisatomi, T.; Katayama, M.; Shibata, N.; Yamada, T.; et al. Efficient hydrogen evolution on (CuInS₂)_x(ZnS)_{1-x} solid solution-based photocathodes under simulated sunlight. *Chem. Commun.* **2019**, *55*, 470–473. [[CrossRef](#)]

42. Zhao, J.; Minegishi, T.; Zhang, L.; Zhong, M.; Gunawan; Nakabayashi, M.; Ma, G.; Hisatomi, T.; Katayama, M.; Ikeda, S.; et al. Enhancement of Solar Hydrogen Evolution from Water by Surface Modification with CdS and TiO₂ on Porous CuInS₂ Photocathodes Prepared by an Electrodeposition–Sulfurization Method. *Angew. Chem. Int. Ed.* **2014**, *53*, 11808–11812. [[CrossRef](#)] [[PubMed](#)]
43. Luo, J.; Tilley, S.D.; Steier, L.; Schreier, M.; Mayer, M.T.; Fan, H.J.; Grätzel, M. Solution Transformation of Cu₂O into CuInS₂ for Solar Water Splitting. *Nano Lett.* **2015**, *15*, 1395–1402. [[CrossRef](#)]
44. Matoba, K.; Matsuda, Y.; Takahashi, M.; Sakata, Y.; Zhang, J.; Higashimoto, S. Fabrication of Pt/In₂S₃/CuInS₂ thin film as stable photoelectrode for water splitting under solar light irradiation. *Catal. Today* **2021**, *375*, 87–93. [[CrossRef](#)]
45. Tanaka, M.; Matsuda, Y.; Takahashi, M.; Higashimoto, S. Photocatalytic water splitting on the CuInS₂ photoelectrodes: Effects of co-electrodeposition mechanisms on the photoelectrochemical properties. *Catal. Today* **2022**, *410*, 302–308. [[CrossRef](#)]
46. Gunawan; Septina, W.; Ikeda, S.; Harada, T.; Minegishi, T.; Domen, K.; Matsumura, M. Platinum and indium sulfide-modified CuInS₂ as efficient photocathodes for photoelectrochemical water splitting. *Chem. Commun.* **2014**, *50*, 8941–8943. [[CrossRef](#)]
47. Chae, S.Y.; Yoon, N.; Joo, O.S.; Park, E.D. Monitoring Transformations of Catalytic Active States in Photocathodes Based on MoS_x Layers on CuInS₂ Using In Operando Raman Spectroscopy. *Angew. Chem.* **2023**, *135*, e202215227. [[CrossRef](#)]
48. Chae, S.Y.; Lee, M.; Je Kim, M.; Cho, J.H.; Kim, B.; Joo, O.-S. p-CuInS₂/n-Polymer Semiconductor Heterojunction for Photoelectrochemical Hydrogen Evolution. *ChemSusChem* **2020**, *13*, 6651–6659. [[CrossRef](#)]
49. Kumar, S.; Yadav, N.; Kumar, P.; Ganguli, A.K. Design and Comparative Studies of Z-Scheme and Type II Based Heterostructures of NaNbO₃/CuInS₂/In₂S₃ for Efficient Photoelectrochemical Applications. *Inorg. Chem.* **2018**, *57*, 15112–15122. [[CrossRef](#)]
50. Liu, Z.; Lu, X.; Chen, D. Photoelectrochemical Water Splitting of CuInS₂ Photocathode Collaborative Modified with Separated Catalysts Based on Efficient Photogenerated Electron–Hole Separation. *ACS Sustain. Chem. Eng.* **2018**, *6*, 10289–10294. [[CrossRef](#)]
51. Liu, Z.; Zhou, M. Co-Modification with Cost-Effective Nickel Oxides and Nickel Sulfides on CuInS₂ Nanosheets Photocathode for Enhanced Photoelectrochemical Performance. *ACS Sustain. Chem. Eng.* **2020**, *8*, 512–519. [[CrossRef](#)]
52. He, Y. *CuInS₂ Thin Films for Photovoltaic: RF Reactive Sputter Deposition and Characterization*; Universitätsbibliothek: Gießen, Germany, 2006.
53. Lee, S.-Y.; Park, B.-O. CuInS₂ thin films deposited by sol–gel spin-coating method. *Thin Solid Films* **2008**, *516*, 3862–3864. [[CrossRef](#)]
54. Yokoyama, D.; Minegishi, T.; Maeda, K.; Katayama, M.; Kubota, J.; Yamada, A.; Konagai, M.; Domen, K. Photoelectrochemical water splitting using a Cu(In,Ga)Se₂ thin film. *Electrochem. Commun.* **2010**, *12*, 851–853. [[CrossRef](#)]
55. Baek, M.; Zafar, M.; Kim, S.; Kim, D.-H.; Jeon, C.-W.; Lee, J.; Yong, K. Enhancing Durability and Photoelectrochemical Performance of the Earth Abundant Ni–Mo/TiO₂/CdS/CIGS Photocathode under Various pH Conditions. *ChemSusChem* **2018**, *11*, 3679–3688. [[CrossRef](#)] [[PubMed](#)]
56. Kumagai, H.; Minegishi, T.; Sato, N.; Yamada, T.; Kubota, J.; Domen, K. Efficient solar hydrogen production from neutral electrolytes using surface-modified Cu(In,Ga)Se₂ photocathodes. *J. Mater. Chem. A* **2015**, *3*, 8300–8307. [[CrossRef](#)]
57. Fan, R.; Mao, J.; Yin, Z.; Jie, J.; Dong, W.; Fang, L.; Zheng, F.; Shen, M. Efficient and Stable Silicon Photocathodes Coated with Vertically Standing Nano-MoS₂ Films for Solar Hydrogen Production. *ACS Appl. Mater. Interfaces* **2017**, *9*, 6123–6129. [[CrossRef](#)]
58. Wang, M.; Chang, Y.-S.; Tsao, C.-W.; Fang, M.-J.; Hsu, Y.-J.; Choy, K.-L. Enhanced photoelectrochemical hydrogen generation in neutral electrolyte using non-vacuum processed CIGS photocathodes with an earth-abundant cobalt sulfide catalyst. *Chem. Commun.* **2019**, *55*, 2465–2468. [[CrossRef](#)]
59. Hasani, A.; Le, Q.V.; Tekalgne, M.; Choi, M.-J.; Lee, T.H.; Jang, H.W.; Kim, S.Y. Direct synthesis of two-dimensional MoS₂ on p-type Si and application to solar hydrogen production. *NPG Asia Mater.* **2019**, *11*, 47. [[CrossRef](#)]
60. Ding, Q.; Meng, F.; English, C.R.; Cabán-Acevedo, M.; Shearer, M.J.; Liang, D.; Daniel, A.S.; Hamers, R.J.; Jin, S. Efficient Photoelectrochemical Hydrogen Generation Using Heterostructures of Si and Chemically Exfoliated Metallic MoS₂. *J. Am. Chem. Soc.* **2014**, *136*, 8504–8507. [[CrossRef](#)]
61. Li, S.; Yang, G.; Ge, P.; Lin, H.; Wang, Q.; Ren, X.; Luo, S.; Philo, D.; Chang, K.; Ye, J. Engineering Heterogeneous NiS₂/NiS Cocatalysts with Progressive Electron Transfer from Planar p-Si Photocathodes for Solar Hydrogen Evolution. *Small Methods* **2021**, *5*, 2001018. [[CrossRef](#)]
62. Sim, Y.; John, J.; Surendran, S.; Moon, B.; Sim, U. Efficient Photoelectrochemical Water Splitting Reaction using Electrodeposited Co₃Se₄ Catalyst. *Appl. Sci.* **2019**, *9*, 16. [[CrossRef](#)]
63. Mora, S.; Romeo, N.; Tarricone, L. Minority carriers lifetime measurements in CuInS₂ by photoelectromagnetic effect. *Solid State Commun.* **1979**, *29*, 155–157. [[CrossRef](#)]
64. Brus, V.V.; Orletsky, I.G.; Ilashchuk, M.I.; Maryanchuk, P.D. Electrical properties of thin-film semiconductor heterojunctions n-TiO₂/p-CuInS₂. *Semiconductors* **2014**, *48*, 1046–1050. [[CrossRef](#)]
65. Broussillou, C.; Savidand, G.; Parissi, L.; Jaime-Ferrer, J.S.; Grand, P.P.; Hubert, C.; Roussel, O.; Saucedo, E.; Bermudez, V.; Andrieux, M.; et al. Rapid thermal processing of CuInSe₂ electroplated precursors for CuIn(S,Se)₂-based thin film solar cells. *Energy Procedia* **2010**, *2*, 9–17. [[CrossRef](#)]
66. Chae, S.Y.; Park, S.J.; Han, S.G.; Jung, H.; Kim, C.-W.; Jeong, C.; Joo, O.-S.; Min, B.K.; Hwang, Y.J. Enhanced Photocurrents with ZnS Passivated Cu(In,Ga)(Se,S)₂ Photocathodes Synthesized Using a Nonvacuum Process for Solar Water Splitting. *J. Am. Chem. Soc.* **2016**, *138*, 15673–15681. [[CrossRef](#)]

67. Jacobsson, T.J.; Fjällström, V.; Edoff, M.; Edvinsson, T. CIGS based devices for solar hydrogen production spanning from PEC-cells to PV-electrolyzers: A comparison of efficiency, stability and device topology. *Sol. Energy Mater. Sol. Cells* **2015**, *134*, 185–193. [[CrossRef](#)]
68. Ishizuka, S.; Okamoto, R.; Ikeda, S. Enhanced Performance of Ternary CuGaSe₂ Thin-Film Photovoltaic Solar Cells and Photoelectrochemical Water Splitting Hydrogen Evolution with Modified p–n Heterointerfaces. *Adv. Mater. Interfaces* **2022**, *9*, 2201266. [[CrossRef](#)]
69. Kim, J.H.; Kaneko, H.; Minegishi, T.; Kubota, J.; Domen, K.; Lee, J.S. Overall Photoelectrochemical Water Splitting using Tandem Cell under Simulated Sunlight. *ChemSusChem* **2016**, *9*, 61–66. [[CrossRef](#)]
70. Frick, J.J.; Cava, R.J.; Bocarsly, A.B. Chalcopyrite CuIn(S_{1-x}Se_x)₂ for Photoelectrocatalytic H₂ Evolution: Unraveling the Energetics and Complex Kinetics of Photogenerated Charge Transfer in the Semiconductor Bulk. *Chem. Mater.* **2018**, *30*, 4422–4431. [[CrossRef](#)]

Disclaimer/Publisher's Note: The statements, opinions and data contained in all publications are solely those of the individual author(s) and contributor(s) and not of MDPI and/or the editor(s). MDPI and/or the editor(s) disclaim responsibility for any injury to people or property resulting from any ideas, methods, instructions or products referred to in the content.